



OPEN Assessment of environmental radioactivity in the City of Melilla

J. G. Rubiano^{1✉}, F. Cámara², N. Miquel-Armengol¹, C. Briones³, C. León-Navarro⁴, M. Añino⁵, H. Alonso¹, A. Tejera¹ & P. Martel¹

There is a significant scarcity of environmental radiological data from the Spanish territories in the North Africa and along the southern Alboran Sea coast. This paper presents the results of environmental radioactivity campaigns conducted between 2010 and 2025 in Melilla to produce a terrestrial gamma radiation map and analyse the distribution of natural radioisotopes (^{226}Ra , ^{232}Th and ^{40}K) and ^{137}Cs in soils. Mean activity concentrations are 22 Bq kg⁻¹ for ^{226}Ra , 24 Bq kg⁻¹ for ^{232}Th , and 305 Bq kg⁻¹ for ^{40}K , all below global medians and Spanish averages. Using these data, a dose model was applied to generate a dose map of the territory. The estimated annual effective dose of 0.23 mSv y⁻¹ is also below the global average, indicating no radiological concern for the population. Due to Melilla's border location and proximity to the Strait of Gibraltar, a characterization of its beaches was performed to establish a baseline for potential external contamination. Several indices established by international regulatory agencies were calculated to quantify radiological risk in outdoor and indoor environments. Finally, a radon potential exposure map was developed to identify areas where buildings could exceed the 300 Bq m⁻³ reference level set by the Building Technical Code in accordance with Council Directive 2013/59/Euratom.

Keywords Environmental radioactivity, Natural radioisotopes, Radon risk, Cesium deposition, Environmental doses

The average annual radiation doses received by humans primarily originate from natural sources, which include external sources such as cosmic radiation and terrestrial radioactive materials, and internal sources, which enter the human body through inhalation and ingestion. The radiation dose from natural sources is influenced by various factors, including geographical location, altitude, and building materials¹. The most significant environmental radioisotopes contributing to natural radiation include members of the ^{238}U decay series (notably ^{222}Rn), the ^{232}Th decay series, and ^{40}K . Additionally, artificial radionuclides such as ^{137}Cs , primarily originating from atmospheric nuclear weapons testing and nuclear accidents, contribute to environmental radioactivity through atmospheric deposition. These factors result in significant variations in natural and anthropogenic radiation levels depending on soil and rock composition, elevation above sea level, climatic conditions, and other environmental parameters².

The regulation of environmental radioactivity in the European Union aims to minimize the risks associated with exposure to ionizing radiation, of both artificial and natural origin. Within this framework, natural radioactivity, particularly exposure to radon gas and naturally occurring radionuclides in soil and water, is a priority due to its impact on public health. To address these risks, the regulations include radiological risk indices that help to assess and manage population exposure. The Council Directive 2013/59/Euratom³ lays down basic safety standards for protection against the dangers arising from exposure to ionizing radiation. It mandates the member states to develop national radon action plans, identifying Radon Priority Areas where it is necessary to prioritise mitigation actions in new and existing buildings. Additionally, it establishes a limit of 300 Bq m⁻³ of indoor radon concentration for the adoption of reference levels by member states in their regulations. The directive also introduces the Global Radiological Hazard Index, based on the concentration of natural radionuclides in soil and building materials, to determine the need for preventive measures. The monitoring of artificial radionuclides, such as ^{137}Cs from atmospheric deposition due to nuclear tests and accidents like Chernobyl, remains a regulated aspect within the European framework, by virtue of Articles 35 and 36 of the Euratom Treaty concerning the monitoring of radionuclides in the environment.

¹Departamento de Física, Universidad de Las Palmas de Gran Canaria, Las Palmas de Gran Canaria, Spain.

²Department of Earth Sciences Ardito Desio, Università degli studi di Milano, Milan, Italy. ³Departamento de Ingeniería Industrial, Universidad de La Laguna, 38200 San Cristóbal de La Laguna, Spain. ⁴IES Primero de Mayo. Consejería de educación, formación profesional y actividad física y deportes del Gobierno de Canarias, Las Palmas de Gran Canaria, Spain. ⁵IES Juan Antonio Fernández Pérez, Ministerio de educación, formación profesional y deportes, Melilla, Spain. ✉email: jesus.garciarubiano@ulpgc.es

Spain has adapted its legislation to European directives, establishing specific regulations for environmental radioactivity with a particular focus on natural radiation. The Spanish Royal Decree 1029/2022 of December 20 regulates health protection against risks derived from exposure to ionizing radiation⁴. It includes specific measures for radon control in workplaces, whereas the measures adopted in new buildings or renovation works in existing buildings are included in the Section HS-6 of the Building Technical Code (CTE)⁵, both aligning with European limits and requiring remedial actions when levels exceed 300 Bq m^{-3} . It also incorporates the use of the Internal and External Radiological Hazard Index, which assesses the impact of natural radionuclides on human health, especially in areas with high concentrations of ^{238}U and ^{232}Th decay series.

The city of Melilla is located in the northeastern Africa, on the southeastern margin of the Iberian Peninsula ($35^{\circ}17'37'' \text{ N}$, $2^{\circ}56'18'' \text{ W}$). As a Spanish territory in the North Africa, it falls under the scope of European Union regulations concerning environmental radioactivity and their transposition into Spanish national legislation. Nevertheless, environmental radioactivity in Melilla, and more broadly along the southern coast of the Alborán Sea where the city lies, has been scarcely investigated to date.

Description of the study area

Melilla has an area of 12.33 km^2 and is arranged in a large semicircle around the beach and the port, with an urban layout covering 9.08 km^2 . According to the most recent data from the National Statistics Institute of Spain (INE), the population of Melilla on January 1, 2024, was 85,811 inhabitants, making it the most densely populated autonomous region in Spain, with 6,960 inhabitants/ km^2 . Likewise, the INE reports that Melilla has a total of 9,448 buildings. Due to its location, it has the character of a southern border zone of the European Union. The approximate length of its border perimeter with the neighbouring kingdom of Morocco is about 11 km, and that of its maritime perimeter is about 9 km. Melilla is in the North African region of Guelaya, on the western coast of the Cape Tres Forcas. At the foot of the promontory stands the Gourougou mountain massif, over 800 m high. The coast of Melilla is bathed by the Alboran Sea, and at its southern end lies the coastal lagoon of Mar Chica.

The territory of Melilla is geographically divided into three parts (Fig. 1a). The northern zone is where the highest elevations are found (130 m above sea level); it contains the Rostrogordo plains and the Tigorfaten stream basin, where the relief is primarily of carbonate origin. These Miocene reliefs reach the sea to the east, forming the rocky cliffs locally known as “Los Cortados”. Continuing from these, on a small limestone promontory about 30 m high that juts out into the sea, are the ancient city, the citadel, and the fortress. To the south is an alluvial plain that forms the current mouth of the Oro River, where the modern city is located. The Quaternary, which extends to the riverbeds found in the central unit, where the Oro River flows, has left behind sedimentary deposits of pebbles, blocks, sand, and silt of very recent age. It also extends to the stretch of coast south of the old town and the port, with a geological substratum of sand and gravel. The third geological unit lies to the southwest, starting from the airport, where the volcanic outcrops of the Gourougou Massif predominate.

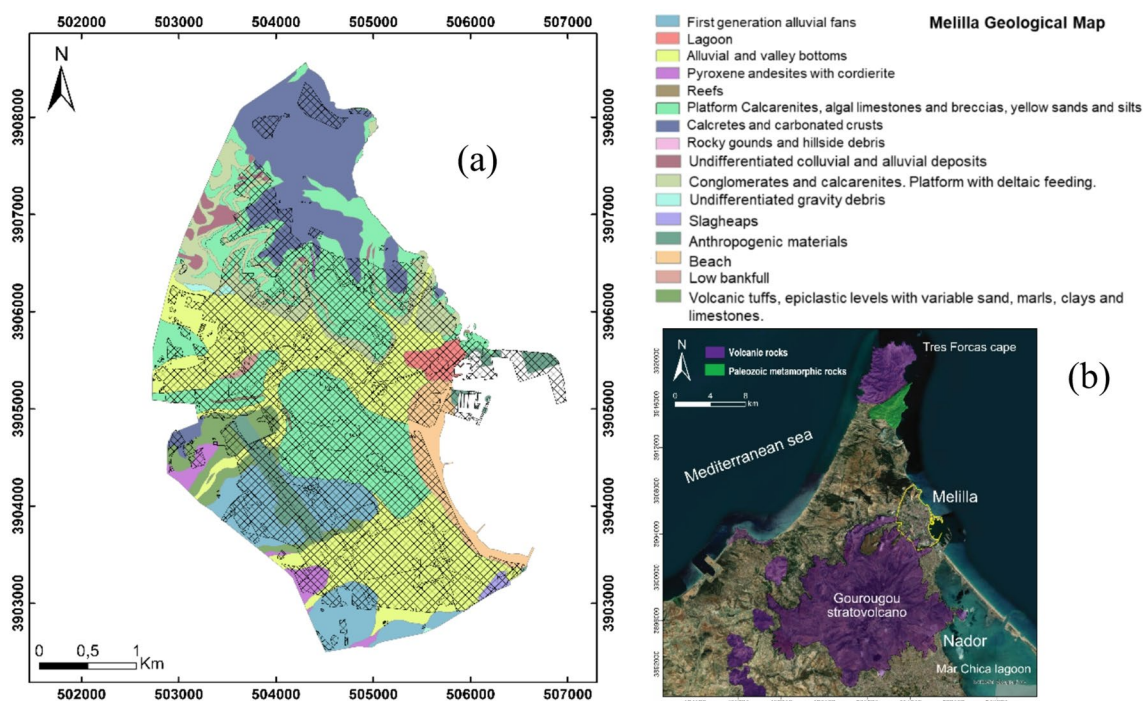


Fig. 1. (a) Geological map of the territory of Melilla. Geological and Continuous Map of Spain (GEODE) Geological and Mining Institute of Spain (IGME). (b) Geological sketch of the Guelaya area surrounding Melilla. Base map data from ArcGIS (Esri, Maxar, Earthstar Geographics, and the GIS user community; ArcGIS release 3.5, <https://www.esri.com/>). Map modified using Affinity Designer 2 (version 2.5.0).

The Neogene magmatic field of the Melilla region includes the Tortonian Trois Fourches volcanic field and the Gourougou volcanic complex (Fig. 1b), which started developing at Tortonian with K-calc-alkaline activity, followed by Messinian Si–K-rich shoshonitic effusive products. The last volcanic activity corresponds to Pliocene ages and alkaline effusive products. The main volcanic building corresponds to the Gourougou stratovolcano, formed in the Messinian period, and includes basaltic trachyandesites, trachyandesites, and andesites, including aerial lava flows and several pumice flows that reach the Neogene basin at the NE^{6–8}.

Geochemically, volcanic Si–K-rich group rocks from Gourougou show enrichment of fluid-mobile elements such as Rb, U, and K relative to less fluid-mobile or fluid-immobile elements (e.g., REE, Nb, and Ta), whereas latter Si-poor lavas show a relative depletion in fluid-mobile elements of Rb, Th, U, K, and Pb compared with less fluid-mobile elements such as REE, Nb, and Ta⁹. The sedimentary rocks cropping out in the northern zone are depleted in K (as well as in Th, U, Rb and Pb), being composed mainly of calcium carbonate with small amount of silicic terrigenous material (including quartz and feldspars). The same situation applies to the alluvial and colluvial deposits coming from the erosion of the Miocene reliefs. When the alluvial material comes from the erosion of volcanic rocks (the south-west part of the autonomous city territory), these mostly contain fragments of altered volcanic material, inheriting their geochemical footprint but diluting them due to the presence of carbonate cements.

This paper presents the results of several field campaigns conducted between 2010 and 2025 in the autonomous city of Melilla, aimed at achieving a comprehensive radiological characterization of its environment. To this end, the distribution of natural radioisotopes (²²⁶Ra, ²³²Th, ²¹⁰Pb and ⁴⁰K) and anthropogenic ¹³⁷Cs in soils was analysed, and the results were correlated with the underlying geology. An assessment of environmental radioactivity in the coastal zone was carried out to characterize the territory under the possible arrival of radioactive pollutants by marine streams. Based on these data, a map of ambient gamma radiation dose was generated and experimentally validated through in situ measurements of terrestrial gamma exposure rates. Subsequently, various dose-risk assessments were carried out, and finally, a radon potential exposure map for the territory was created in accordance with the guidelines of the Spanish Nuclear Safety Council.

Results

Activity concentration of natural radioisotopes and ¹³⁷Cs in soils

For the sampling and subsequent analysis of the radioisotope composition of soils in Melilla, the geological map presented in Fig. 1 was simplified by reorganizing the geological units according to their dominant lithological characteristics. This simplification reduced the geological framework to three primary categories: volcanic rocks (VR unit), sedimentary rocks (SR unit, predominantly carbonates), and Quaternary deposits. The latter were further subdivided into two lithologically distinct groups: Qa, comprising alluvial and colluvial sediments, and Qb, consisting of alluvial fans mainly derived from volcanic materials. Figure 2a shows the resulting lithology-based classification and the corresponding grid of sampling points for radioisotope analysis in soils (circles). Since most of the area is urbanized, samples were collected only in locations where the natural soil is exposed; consequently, a completely regular sampling grid could not be achieved. Environmental gamma-radiation measuring points are represented by triangles. Sampling of all four defined lithological units was conducted to the extent permitted by local constraints, as a substantial portion of the territory is urbanized and several areas are located within restricted-access zones associated with official installations.

A total of 27 samples of soil were analysed by high resolution gamma spectroscopy to determine the specific activities of ²²⁶Ra, ²³²Th, ⁴⁰K, ²¹⁰Pb and ¹³⁷Cs. Table 1 reports the descriptive statistics of the main results. The activity concentrations, expressed in Bq kg⁻¹, range from 64 ± 8 to 670 ± 30 with a mean value of 305 ± 17 for ⁴⁰K; from 4 ± 2 to 73 ± 5 with a mean value of 24 ± 2 for ²³²Th; and from 10 ± 2 to 56 ± 5 with a mean value of 22 ± 2 for ²²⁶Ra.

Terrestrial gamma dose rates at 1 m

Exposure rates were measured at 47 locations across the study area, and terrestrial gamma dose rates (TGR) were derived by subtracting the cosmic-ray contribution following the procedure described in the Material and methods section. The resulting TGR exhibit an arithmetic mean of 47 nGy h⁻¹, with maximum values of 172 nGy h⁻¹ in areas dominated by volcanic lithologies, and values close to the cosmic radiation background along the beach zones.

Discussion

Correlation of soil radioisotopes with lithology

Figure 2b,d show the contour maps of activity concentrations of ²²⁶Ra, ²³²Th (²²⁸Ra), and ⁴⁰K. In general, there is a close relationship between the activity concentrations of radioisotopes and the nature of the rocks that predominate in the terrain. Thus, low concentration rates are recorded in most of the territory, consistent with the presence of carbonate rocks and siliciclastic deposits with low concentrations of K, heavy elements, and therefore also radioisotopes. The lowest values are found in the northern part of the territory, which has also the highest elevation (plains and pine forests of Rostrogordo). Higher values, up to 40 Bq kg⁻¹ of ²²⁶Ra and 500 Bq kg⁻¹ of ⁴⁰K, are found in the southwest area near the airport, where volcanic rocks (trachyandesites and andesites) with a higher presence of heavy trace elements outcrop, albeit in a small area.

According to UNSCEAR 2000 (Annex B, Table 5)¹, the worldwide median activity concentrations in soils are approximately 35 Bq kg⁻¹ for ²²⁶Ra, 30 Bq kg⁻¹ for ²³²Th, and 400 Bq kg⁻¹ for ⁴⁰K, with typical worldwide variation ranges of 17–60 Bq kg⁻¹, 11–64 Bq kg⁻¹, and 140–850 Bq kg⁻¹, respectively. For soils in Spain, UNSCEAR¹ reports the mean activity concentrations of 32 Bq kg⁻¹ for ²²⁶Ra (range 6–250 Bq kg⁻¹), 33 Bq kg⁻¹ for ²³²Th (range 2–210 Bq kg⁻¹), and 470 Bq kg⁻¹ for ⁴⁰K (range 25–1650 Bq kg⁻¹). In our study area (Melilla),

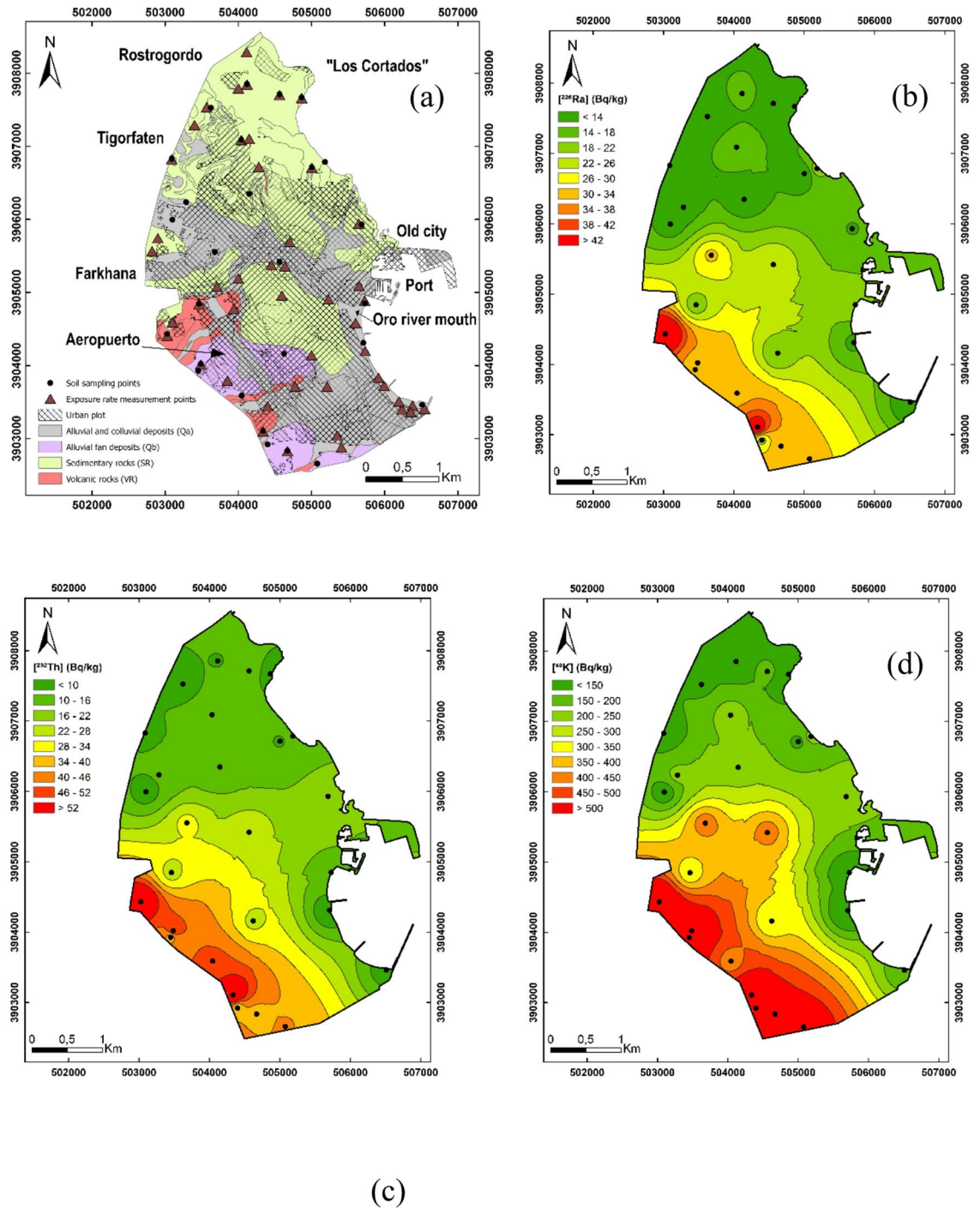


Fig. 2. (a) Simplified geological map of the territory of Melilla. Geological and Continuous Map of Spain (GEODE) Geological and Mining Institute of Spain (IGME) and the location of soil sampling (circles) and exposure rate measurement (triangles) points. (b) ^{226}Ra activity concentration map. (c) ^{232}Th activity concentration map. (d) ^{40}K activity concentration map. Maps generated using ArcGIS Pro software, version 3.5 (ESRI, 2024; <https://www.esri.com/en-us/arcgis/products/arcgis-pro/overview>).

the measured values are 22 Bq kg^{-1} for ^{226}Ra , 24 Bq kg^{-1} for ^{232}Th , and 305 Bq kg^{-1} for ^{40}K , which are below the global medians and the Spanish mean values, and lie in the lower half of the reported ranges for both Spain and the world. These results indicate that the natural radioactivity of the soils in Melilla is comparatively low relative to both national and global contexts, suggesting that terrestrial gamma radiation levels from naturally occurring radionuclides in this area are unlikely to be elevated.

Figure 3 presents box-and-whisker plots illustrating the distribution of ^{226}Ra , ^{232}Th , and ^{40}K activity concentrations across four lithological groups defined: volcanic rocks (VR unit), sedimentary rocks (SR unit),

	²²⁶ Ra	²³² Th	⁴⁰ K	¹³⁷ Cs	²¹⁰ Pb
Number of samples	27	27	27	15	10
Mean ± standard deviation (Bq kg ⁻¹)	22 ± 12	24 ± 19	300 ± 200	5 ± 3	19 ± 19
Max (Bq kg ⁻¹)	56 ± 5	75 ± 4	670 ± 30	13 ± 1	87 ± 12
Min (Bq kg ⁻¹)	10 ± 2	4 ± 2	64 ± 8	0.8 ± 0.5	15 ± 6

Table 1. Activity concentration of natural radioisotopes and ¹³⁷Cs in surface soils of Melilla.

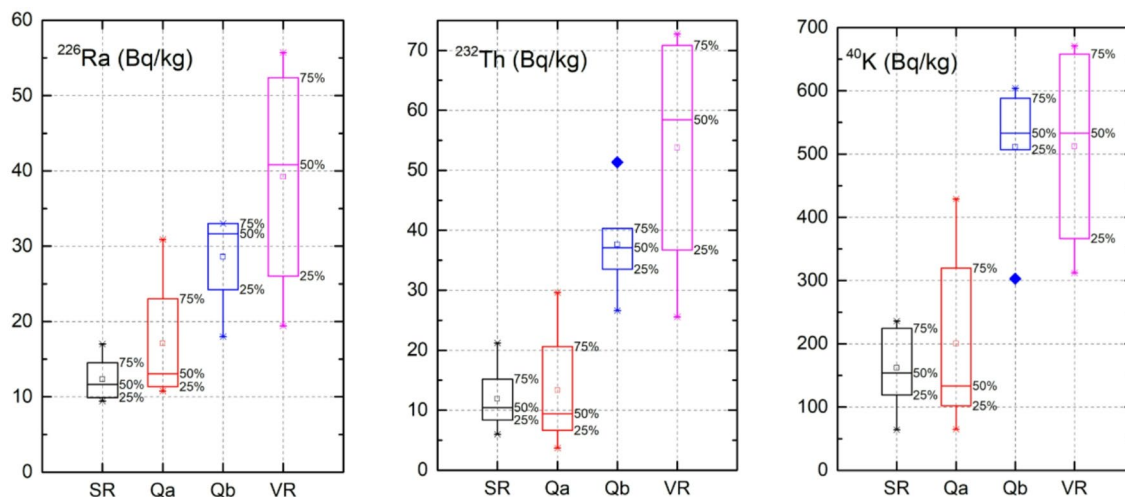


Fig. 3. Box-and-whisker diagrams of the activity concentrations of natural radioisotopes classified according to the different lithotypes. Black SR, red Qa, blue Qb and magenta VR.

predominantly carbonates), Quaternary alluvial and colluvial deposits (Qa), and Quaternary alluvial fans mainly derived from volcanic materials (Qb).

Figure 3 shows that two distinct lithological groups can be distinguished based on natural radioisotope activity concentrations in soils. The first group includes sedimentary rocks (SR), which exhibit median values of 12 Bq kg⁻¹ for ²²⁶Ra, 154 Bq kg⁻¹ for ⁴⁰K, and 10 Bq kg⁻¹ for ²³²Th, together with Quaternary alluvial deposits (Qa), which show very similar values of 13 Bq kg⁻¹ for ²²⁶Ra, 134 Bq kg⁻¹ for ⁴⁰K, and 9 Bq kg⁻¹ for ²³²Th. The second group comprises volcanic rocks (VR) and volcanic alluvial deposits (Qb). Volcanic rocks (VR) display median values of 41 Bq kg⁻¹ for ²²⁶Ra, 533 Bq kg⁻¹ for ⁴⁰K, and 58 Bq kg⁻¹ for ²³²Th, whereas Qb deposits present median values of 32 Bq kg⁻¹ for ²²⁶Ra, 533 Bq kg⁻¹ for ⁴⁰K, and 37 Bq kg⁻¹ for ²³²Th. Mann–Whitney U tests performed between the two groups (VR + Qb vs. SR + Qa) revealed highly significant differences for all three radioisotopes ($p < 0.001$), indicating pronounced contrasts in their distributions.

A denser sampling network, including the Moroccan border where the volcanic lithologies of the Gourougou Massif predominate, could reveal local variations in natural radioactivity levels in the southwest of the city, reflecting the presence of silicon-potassium or silicon-sodium-rich rocks. While most volcanic rocks in Melilla are silicon-poor alkaline basalts, potassium-rich trachyandesites outcropping in the Farkhana area west of the city may contain, on average, nearly twice the ²³²Th and ²²⁶Ra concentrations.

Atmospheric deposition of ¹³⁷Cs and ²¹⁰Pb

Soil radioisotope analyses were also employed to investigate the presence of the artificial radioisotope ¹³⁷Cs. This radioisotope was generated primarily during nuclear weapons tests carried out throughout 20th century¹⁰ and the accidents at the Chernobyl¹¹ and Fukushima¹² nuclear power plants. The global distribution of ¹³⁷Cs is controlled by both stratospheric injections of the isotope and atmospheric circulation patterns. ¹³⁷Cs injected into the stratosphere descends to the troposphere, primarily at mid- and polar latitudes, and subsequently precipitates onto the Earth's surface in both wet and dry forms (the so-called “fallout”). ¹³⁷Cs is commonly used as a tracer for assessing soil erosion and redistribution processes due to its well-characterized fallout history and strong adsorption to soil particles^{13,14}.

Figure 4a shows the distribution map of ¹³⁷Cs in the Melilla region. As can be seen, it peaks in the northern zone, where the only forested region in the study area is located. This is an area with less urban pressure and, logically, less soil erosion due to human activity.

To analyze this result, Fig. 4b shows the distribution of another naturally occurring environmental tracer, ²¹⁰Pb. This radioisotope originates from ²²⁶Ra, which decays to ²²²Rn, which, as a gas, continuously diffuses into the atmosphere. One of the offspring of ²²²Rn is ²¹⁰Pb, which is therefore also found naturally in the atmosphere. Thus, there are two distinct contributions related to the ²¹⁰Pb activity present in surface soil samples. The first

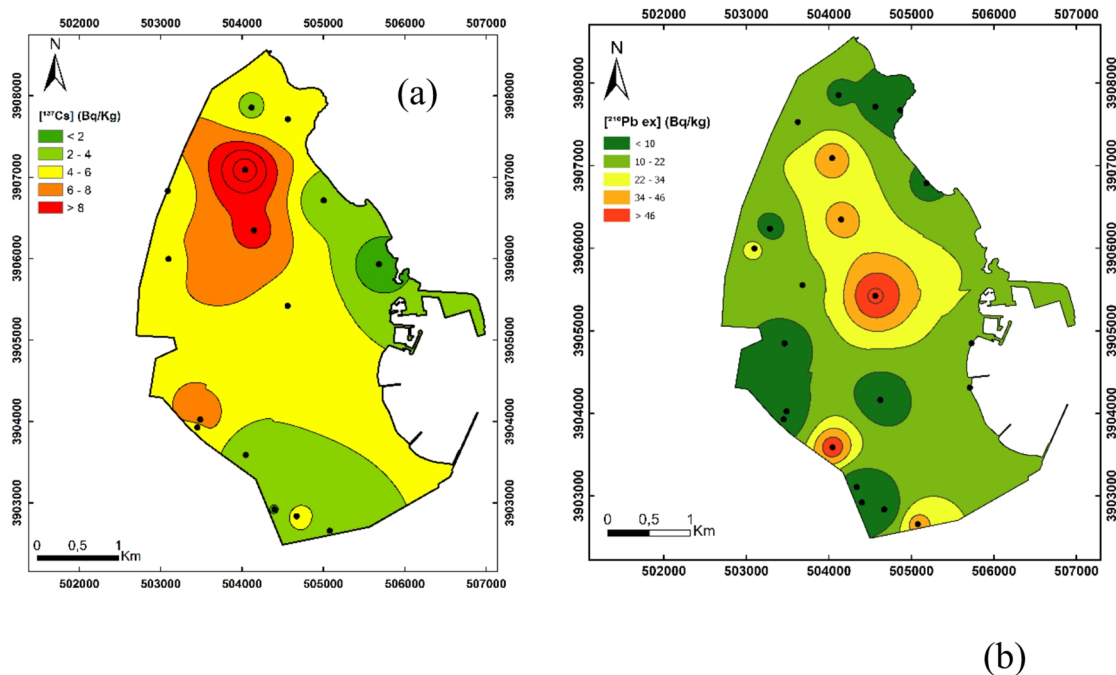


Fig. 4. (a). Activity concentration of ^{137}Cs in topsoils (b) Activity concentration of $^{210}\text{Pb}_{\text{ex}}$ in topsoils. Maps generated using ArcGIS Pro software, version 3.5 (ESRI, <https://www.esri.com/en-us/arcgis/products/arcgis-pro/overview>).

originates from the concentration of ^{210}Pb precursor radioisotopes (^{226}Ra) in the soil. The concentration of ^{210}Pb from this source is called “supported ^{210}Pb ”. The second contribution to ^{210}Pb in soils, originating from the decay of ^{222}Rn released into the atmosphere¹⁵, represents a smaller component compared with the primary source. The subsequent incorporation of the latter into soils through dry deposition or wet precipitation produces an “excess” of this radioisotope in relation to the activity concentration of ^{226}Ra present in the soil. Therefore, ^{210}Pb from this origin is known as “unsupported ^{210}Pb ” or “excess ($^{210}\text{Pb}_{\text{ex}}$)”. Because of its atmospheric origin, this excess lead has a similar dynamic to ^{137}Cs ; therefore, it is also widely used as a natural radiotracer in erosion processes^{13,16,17}.

Table 1 shows the ranges of values for the measured data for ^{137}Cs and ^{210}Pb . In some samples, the measured concentrations of these radioisotopes were below the detection limit of the equipment, as indicated in Table 1. Figure 4b shows the distribution of $^{210}\text{Pb}_{\text{ex}}$ in the territory, which follows a pattern like that of ^{137}Cs , with maxima located in areas with less anthropogenic pressure in the northern part of the city. Nevertheless, in the case of $^{210}\text{Pb}_{\text{ex}}$, additional maxima appear in the centre of the territory. One is near an industrial area, where the city’s fuel depots are located, and another is near the airport, where aviation fuel depots are located and exhaust products from outgoing flights are deposited daily. Car or plane exhausts release fine particulates (aerosols) which can act as carriers for ^{210}Pb in the atmosphere, enhancing its transport and deposition^{18,19}. This could indicate a possible anthropogenic origin for these maxima.

Radioisotope study of beaches in the coastal zone

This radioisotope study of the coastal zone is important for establishing a baseline of coastal radioactivity. This will allow for the detection of possible deviations due to marine contaminants, which is important given that the city is located near a densely populated area with industrial and agricultural activity. Furthermore, the Alboran Sea is one of the areas in the world with the highest volume of vessel traffic passing through the Strait of Gibraltar.

Samples were taken from the sandy beaches of the city’s inner bay, bordered by the seawalls of the port of Melilla and the breakwater of the Moroccan port of Nador. The bay beaches are separated into two zones by the mouth of the Oro River. Due to their location, these beaches are subject to high anthropogenic pressure and are regularly cleaned and replenished by the city’s environmental authorities. The artificial beach of “Horcas Coloradas” in the northern part of the territory was also sampled. This beach is exposed to the open sea, although it has a small breakwater. It occupies the site where the city’s garbage dump was located for decades. The site was later reclaimed and converted into a beach.

The activity concentrations of ^{40}K , ^{228}Ra , and ^{226}Ra measured at the sampling points along Melilla beaches, expressed in Bq kg^{-1} , range from 32 ± 7 to 420 ± 20 with a mean value of 160 ± 10 for ^{40}K ; from 2 ± 1 to 37 ± 2 with a mean value of 10 ± 2 for ^{228}Ra ; and from 5.3 ± 0.7 to 42 ± 2 with a mean value of 13.1 ± 0.9 for ^{226}Ra . Interpolation maps of the activity concentrations of natural radioisotopes at the sampling points along Melilla beaches, created by ArcGIS software²⁰, are shown in Fig. 5. These activity concentrations show clear contrasts between the geological units (Qa + SR and Qb + VR) and the coastal sands (Bay beaches and Horcas Coloradas beach). For ^{226}Ra , Qb + VR shows the highest mean activity ($33 \pm 12 \text{ Bq kg}^{-1}$), followed by Horcas Coloradas

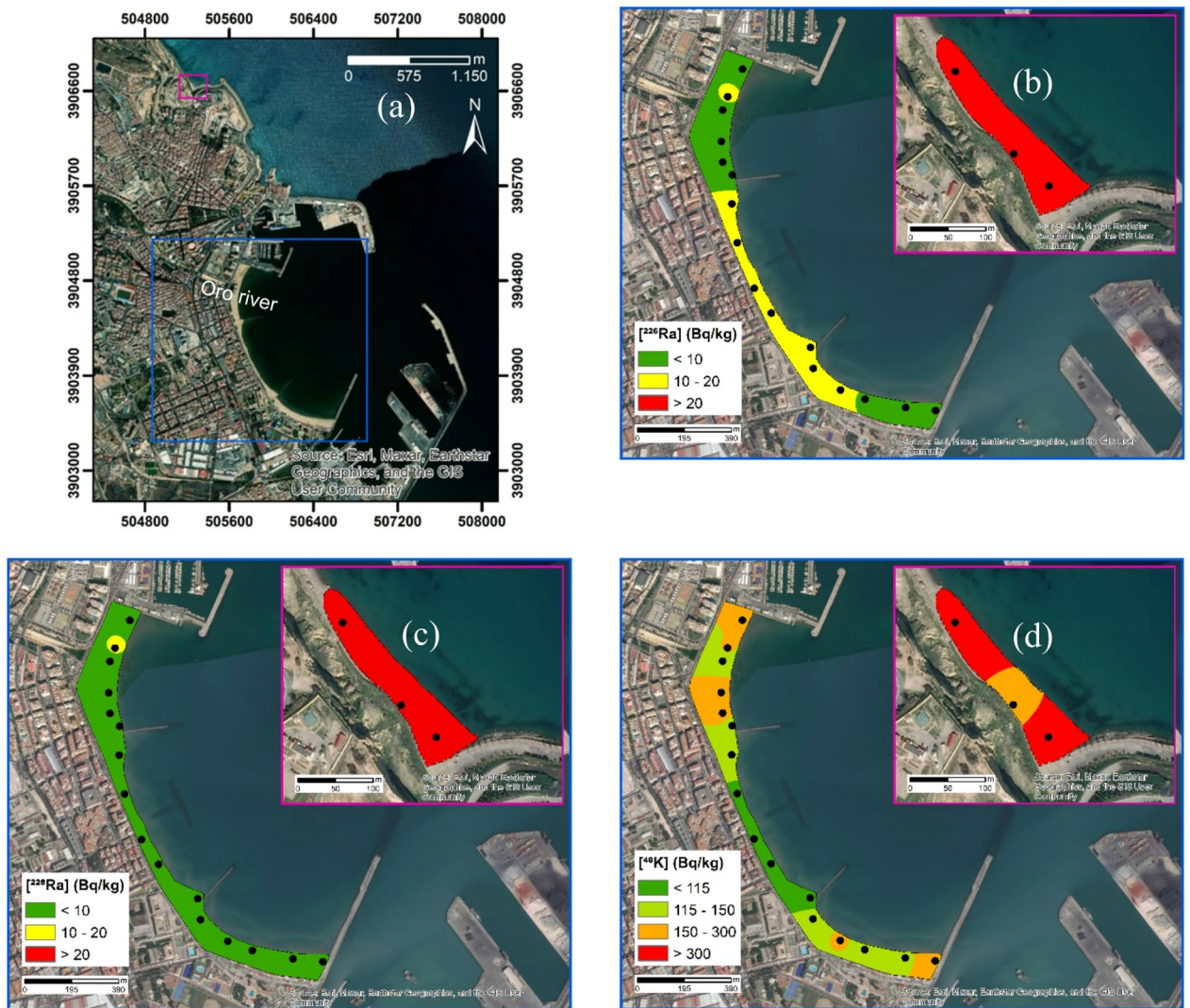


Fig. 5. (a) Map of the territory of Melilla. Source: Esri, Maxar, Earthstar Geographics and the GIS user community (b) ^{226}Ra activity concentration (c) ^{228}Ra activity concentration and (d) ^{40}K activity concentration maps on the city beaches. Map generated using ArcGIS Pro software, version 3.5 (ESRI²⁰, <https://www.esri.com/en-us/arcgis/products/arcgis-pro/overview>).

($28 \pm 4 \text{ Bq kg}^{-1}$), whereas Qa + SR ($15 \pm 6 \text{ Bq kg}^{-1}$) and the Bay beaches ($10.3 \pm 1.8 \text{ Bq kg}^{-1}$) exhibit markedly lower values. A similar pattern is observed for ^{40}K : Qb + VR presents the greatest enrichment ($510 \pm 130 \text{ Bq kg}^{-1}$), intermediate values occur in Horcas Coloradas beach ($317 \pm 30 \text{ Bq kg}^{-1}$), and considerably lower activities characterize Qa + SR ($180 \pm 110 \text{ Bq kg}^{-1}$) and the Bay beaches ($134 \pm 33 \text{ Bq kg}^{-1}$). For ^{232}Th , Qb + VR again records the highest concentrations ($44 \pm 16 \text{ Bq kg}^{-1}$), followed by Horcas Coloradas beach ($24.7 \pm 1.0 \text{ Bq kg}^{-1}$), whereas Qa + SR ($13 \pm 8 \text{ Bq kg}^{-1}$) and the Bay beaches ($7.7 \pm 1.9 \text{ Bq kg}^{-1}$) show the lowest levels. Overall, Qb + VR is consistently enriched in all three radionuclides compared with Qa + SR and beach sediments, while Horcas Coloradas beach systematically exhibits higher activities than the Bay Beaches.

As can be seen, the beaches of the bay show a low concentration of radioisotopes compared to the maximum concentrations found in the interior. On the central beaches of the bay, certain differences in the behavior of ^{226}Ra and ^{40}K can be observed. This may be because these beaches were artificially constructed in the 1980s using sand from the surrounding seabed, while the beaches at the ends of the coastline formed naturally through sedimentation by marine currents. Higher levels of natural radioisotopes are found at the Horcas Coloradas artificial beach, which may be due to the different origins of the sediments in the area and the influence of the old landfill. In this regard, remains of ceramic construction materials persist in the form of pebbles in the sands.

Outdoor and indoor gamma absorbed dose rates in air

There are two main radiological effects derived from radioactivity in soils that justify the importance of measuring them. The first is internal irradiation of the lungs by progeny of ^{222}Rn . The second is external irradiation of the body by gamma rays emitted from radionuclides in situ. In the case of external irradiation,

	\dot{D}_{out} (nGy h ⁻¹)	\dot{D}_{in} (nGy h ⁻¹)	\dot{H}_{out} (mSv y ⁻¹)	\dot{H}_{in} (mSv y ⁻¹)	$ELCR_{out}$	$ELCR_{in}$
Mean	37	71	0.05	0.18	1.6×10^{-4}	6.4×10^{-4}
SD	25	47	0.03	0.12	1.1×10^{-4}	4.3×10^{-4}
Max	95	182	0.12	0.47	4.2×10^{-4}	1.6×10^{-3}
Min	11	21	0.01	0.05	3.5×10^{-5}	1.8×10^{-4}

Table 2. Ambient gamma dose, annual equivalent dose and excess lifetime cancer risk (ELCR).

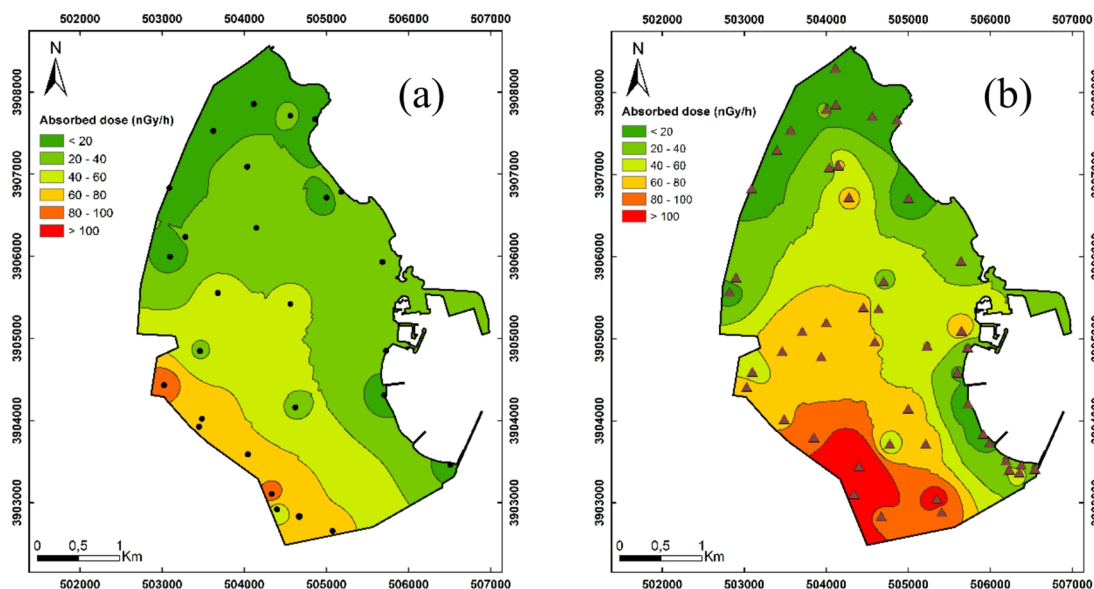


Fig. 6. (a). Absorbed dose rate map obtained from the dose conversion factors of UNSCEAR²⁴ (b) Absorbed dose rate map obtained from in situ gamma measurements. Maps generated using ArcGIS Pro software, version 3.5 (ESRI²⁰, <https://www.esri.com/en-us/arcgis/products/arcgis-pro/overview>).

numerous authors have developed mathematical expressions to calculate the absorbed dose rate in air based on the concentrations of the most significant gamma-emitting radionuclides present in the terrain^{1,21–23}. This allows for the determination of the ambient gamma radiation level based on the geological composition of the terrain and the prediction of its possible values based on the concentrations of radioactive materials present. These relationships allow for a rapid assessment of possible contributions of non-natural origin to ambient radiation levels. In this paper, the dose conversion factors proposed by UNSCEAR²⁴ were used to obtain the absorbed dose using the following expression²⁵:

$$\dot{D}_{out} \text{ (nGy h}^{-1}\text{)} = 0.462A_{Ra-226} + 0.604A_{Th-232} + 0.0417A_{K-40} \quad (1)$$

The gamma radiation dose rate in indoor air (\dot{D}_{in}) can be estimated considering a conventional room-sized 4 × 5 × 2.8 m limited by walls with an average thickness of 200 mm and based on the activity concentrations of ²²⁶Ra, ²³²Th, and ⁴⁰K using Eq. (2)

$$\dot{D}_{in} \text{ (nGy h}^{-1}\text{)} = 0.92A_{Ra-226} + 1.1A_{Th-232} + 0.081A_{K-40} \quad (2)$$

Table 2 shows the results. Outdoor dose rates vary from 11 ± 2 nGy h⁻¹ to 96 ± 7 nGy h⁻¹, with an average dose rate for the city of 38 ± 3 nGy h⁻¹. This value is below the cut-off value of 66 nGy h⁻¹ established by García-Talavera et al.²⁶. According to this author, after screening based on TGR, regions with doses below 66 nGy h⁻¹ are not considered priority action areas in terms of radon exposure²⁶. Indoor doses are logically higher and vary from 21 ± 3 nGy h⁻¹ to 182 ± 12 nGy h⁻¹. The average dose for indoor gamma radiation is 71 ± 5 nGy h⁻¹, double of the outdoor dose.

Figure 6a shows the terrestrial outdoor gamma absorbed dose rate (TGDR) contour map obtained by IDW interpolation from the data obtained by applying Eq. (1). Figure 6b presents the experimental TGDR map obtained by in situ measurement of the exposure rate at 1 m from the ground.

As can be observed, both maps qualitatively coincide in detecting the areas with the highest and lowest absorbed dose rates. The observed differences may be due to the uncertainties of the dosimetry model

used and the influence of construction materials in urbanized areas, which can affect the gamma radiation background. Furthermore, the sampling carried out for the gamma measurement is limited by the difficulty of finding sufficiently large areas without urbanization or buildings for an adequate assessment of the gamma component due solely to soil materials. Despite this, Fig. 6a and b show a plausible explanation to the registered environmental gamma radiation that is directly related to the nature of the rocks outcropping in the town: low doses are registered at most of the territory of the town in agreement with the outcropping of carbonate rocks and detrital siliciclastic and carbonate alluvial deposits containing low natural radioactivity. The highest dose values are registered at SW of the town, where Si-K rich volcanic rocks related to Gourougou stratovolcano and quaternary undifferentiated sediments with higher contents of volcanic clasts crop out.

The annual effective dose rate equivalent estimates the annual radiation dose received by an individual from exposure in a natural environment. It considers the exposure duration and the dose conversion factor. To estimate the annual effective outdoor dose, we apply an exposure duration factor of 0.2, assuming the time spent outdoors is around 20% (Eq. 3); to estimate the annual effective indoor dose, we apply a factor of 0.8, assuming the time spent indoors is around 80% (Eq. 4):

$$\dot{H}_{out} \text{ (mSv y}^{-1}\text{)} = \dot{D}_{out} \times 8760 \times 0.2 \times 0.7 \times 10^{-6} \quad (3)$$

$$\dot{H}_{in} \text{ (mSv y}^{-1}\text{)} = \dot{D}_{in} \times 8760 \times 0.8 \times 0.7 \times 10^{-6} \quad (4)$$

where \dot{D} is the absorbed dose rate in nGy h^{-1} , 8,760 is the number of hours in a year, and 0.7 Sv/Gy is the conversion coefficient from absorbed dose to effective dose. Therefore, to obtain the total annual effective dose rate, Eq. (5) may be used:

$$\dot{H}_{tot} \text{ (mSv y}^{-1}\text{)} = \dot{H}_{out} + \dot{H}_{in} \quad (5)$$

Table 2 shows the average annual equivalent outdoor dose due to environmental gamma radiation received by the population, which is 0.18 mSv y^{-1} . The maximum value of 0.47 mSv y^{-1} corresponds to the southwest area of the city, while the minimum values of 0.01 mSv y^{-1} are found in the northern area. The total average annual effective dose rate was estimated to be 0.23 mSv y^{-1} , which is lower than the global average of 0.52 mSv y^{-1} and well below than the 1 mSv y^{-1} limit established by Spanish legislation (Decree 1029/2022) and by ICRP-60 for the environmental dose for the general public^{4,27}.

1. Excess lifetime cancer risk (ELCR).

The possibility of suffering lung cancer due to exposure to natural radioactivity depends on the annual effective dose (outdoor and indoor), as well as the individual life expectancy (set at 70 years for this study) and a risk factor (fatal cancer risk factor per Sievert) of 0.05 Sv^{-1} , See Eqs. (6) and (7):

$$ELCR_{out} = \dot{H}_{out} \times 70 \times 0.05 \quad (6)$$

$$ELCR_{in} = \dot{H}_{in} \times 70 \times 0.05 \quad (7)$$

Consequently, to estimate the total lifetime cancer risk, Eq. (8) must be applied:

$$ELCR_{tot} = ELCR_{out} + ELCR_{in} \quad (8)$$

The ELCR for outdoor gamma exposure takes values ranging from 3.5×10^{-5} to 4.2×10^{-4} with a mean value of 1.6×10^{-4} . For indoor exposure, the values increase by a factor of approximately 4.5, going from 1.8×10^{-4} to 1.6×10^{-3} with a mean value of 6.4×10^{-4} . The total average ELCR obtained as the sum of the average indoor and outdoor contributions is 8×10^{-4} , which is below the global average²⁹ of 1.45×10^{-3} .

Map of potential radon exposure

A Radon Potential Exposure (RPE) map for the territory of Melilla was developed using TGR dose as the decision parameter. Categories of RPE were defined according to gamma radiation intervals established by the Spanish Nuclear Safety Council (CSN) for radon exposure, considering the reference level of 300 Bq m^{-3} set by current regulations^{4,5}. Following García-Talavera et al.²⁶, the proposed Intervals are: Category 0, below 66 nGy h^{-1} ; Category 1, $66\text{--}123 \text{ nGy h}^{-1}$; and Category 2, above 123 nGy h^{-1} .

As reported by García-Talavera et al.²⁶, TGR levels below 66 nGy h^{-1} (Category 0) provide a reliable criterion for including an area from being classified as a Radon Priority Area. This indicates that, with 90% probability, the indoor radon concentration (IRC) measured in a representative building within these areas would remain below the reference level^{30,31}. Thus, the limit of 66 nGy h^{-1} allows a conservative margin that guarantees areas with low radon exposure in buildings, whereas areas with TGR greater than 66 nGy h^{-1} (categories 1 and 2) could report values of IRC greater than reference level of 300 Bq m^{-3} and therefore be classified as radon priority areas³². The resulting RPE map is shown in Fig. 7.

The Map of Potential Radon Exposure indicates that 70.5% of Melilla's urban area (6.40 km^2), particularly in the north and east, falls within Category 0. In contrast, the southwestern part, where volcanic lithology predominates, is classified as Categories 1 and 2. The Spanish Building Code (CTE)⁵, through its Basic Health Document HS-6, mandates specific radon protection measures in areas designated as having non-negligible radon exposure potential. For new buildings, as well as for certain renovations, extensions or changes of use, HS-6 requires the implementation of construction solutions such as protective gas-barriers, ventilated sub-slab

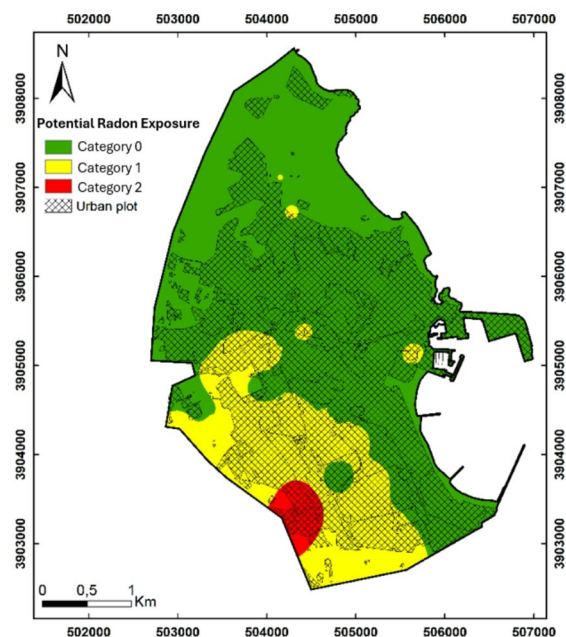


Fig. 7. Radon Potential Exposure (RPE) map of Melilla. Green: Category 0 (below 66 nGy h^{-1}); yellow: Category 1 ($66\text{--}123 \text{ nGy h}^{-1}$); and red: Category 2 (above 123 nGy h^{-1}). Maps generated using ArcGIS Pro software, version 3.5 (ESRI²⁰, <https://www.esri.com/en-us/arcgis/products/arcgis-pro/overview>).

cavities, or soil depressurization systems to limit the ingress of radon from the ground. It is estimated that approximately 2,787 buildings situated in areas classified under these categories would be affected by this regulation. This estimate is based on applying the proportion of territory classified as Categories 1 and 2 to the total number of buildings in Melilla and should be considered approximate.

The results suggest that areas of Melilla classified as Categories 1 and 2, characterized by terrestrial gamma radiation levels above 66 nGy h^{-1} , should undergo indoor radon measurement campaigns in dwellings and workplaces. Such measurements are necessary to accurately assess radon potential in accordance with the guidelines established by the Spanish Building Code (CTE-HS-6) for Radon Priority Areas.

Conclusions

The present investigation has provided for the first time detailed environmental radiological data from the Melilla territory. This study highlights a strong relationship between natural radioisotope concentrations in soils and the predominant lithologies of Melilla. Low activity levels are generally associated with carbonate and siliclastic deposits in the northern highlands, while higher concentrations occur in localized southwestern areas dominated by volcanic rocks. Statistical analysis confirms significant differences between these lithological groups, reflecting marked contrasts in the distribution of ^{226}Ra , ^{232}Th , and ^{40}K . The mean activity concentrations in soils are 22 Bq kg^{-1} for ^{226}Ra , 24 Bq kg^{-1} for ^{232}Th , and 305 Bq kg^{-1} for ^{40}K , which are below the global medians (35 , 30 , and 400 Bq kg^{-1} , respectively) and the Spanish mean values (32 , 33 , and 470 Bq kg^{-1} , respectively). These results indicate that natural radioactivity and terrestrial gamma radiation levels in Melilla are comparatively low and not elevated relative to national or global contexts.

The distribution of $^{210}\text{Pb}_{\text{ex}}$ closely follows that of ^{137}Cs , with maxima in less urbanized northern zones, but additional peaks are observed near industrial areas, fuel depots, and the airport, indicating localized anthropogenic contributions. Coastal sediments generally exhibit low radioactivity, although variations on artificially constructed beaches suggest influences from sediment origin and residual landfill materials.

Outdoor gamma dose rates across the city are generally low, while indoor levels are higher due to accumulation and confinement within buildings; nonetheless, both remain below national and international regulatory thresholds. Estimated annual effective doses (0.23 mSv y^{-1}) and lifetime cancer risks (8×10^{-4}) are below global averages, indicating no immediate radiological concern for the population.

Potential radon exposure mapping identifies most urban areas as Category 0 in relation to radon potential exposure, while southwestern volcanic zones show elevated potential, corresponding to higher terrestrial gamma radiation (classified as Category 1 and 2). These findings emphasize the need for targeted indoor radon measurements in higher-risk areas to comply with the Spanish Building Code and ensure adequate protection for residents.

Materials and methods

Collection and preparation of soil samples

The methodology followed during soil sampling and gamma radiation measurement was recommended by the MARNA Project of the Nuclear Safety Council^{33–35} in the Guideline CSN-CIT-11.2003c. For data collection, the territory of the autonomous city was divided into ten sectors, and the exposure rate was measured in each area. Given the geometric configuration of the territory (almost a semicircle), a grid of equally spaced radial points was chosen, with the centre at the midpoint of the coastline, where the 16th century Old City is located.

A total of 79 soil and intertidal sediment samples were collected, to represent the diversity of geological soil types and account for potential influence of seasonal maritime changes on the sediments. At each sampling point, a 1 m² area was marked, and superficial sand samples were collected from the top 0–5 cm of soil after being homogenized in situ. Following the established protocol^{36,37}, each sample was labelled and referenced with its GPS geographic location. In the laboratory, the soil samples were subjected to a drying process for 48 h in an oven at 80 °C. They were homogenized by passing through a calibrated 1 mm sieve and hermetically sealed in a plastic container for at least 4 weeks before the measurement to achieve equilibrium between the ²²⁶Ra and ²²⁸Ra series and their progeny. Given the low chemical mobility in soil and sediment, secular equilibrium between ²³²Th and ²²⁸Ra was assumed.

High resolution gamma spectrometry analysis

The determination of radioisotope concentrations by gamma spectrometry was carried out using a coaxial Bertin/Canberra extended range (XtRa) HPGe detector with 40% relative efficiency and a FWHM of 1.1 keV (for 88 keV), shielded in a 15 cm thick iron shield, and connected to a Canberra multichannel analyser model DSA 1000. The efficiency calibration was performed using the Betin/Canberra LABSOC code³⁸ based on the Monte Carlo method, which allows for modelling different sample geometries and obtaining the efficiency curves. For each sample, activity concentration of the natural radioisotopes ²²⁶Ra, ²³²Th, and ⁴⁰K were determined considering the assumption on secular equilibrium. Thus, ²²⁶Ra was determined from ²¹⁴Pb, using the 351.9 keV emission line (intensity 37.6%), and ²¹⁰Pb was directly measured using the emission line of 46.5 keV. Moreover, the unsupported or excess ²¹⁰Pb (²¹⁰Pb_{ex}) was calculated from the activity concentrations of ²¹⁰Pb and ²²⁶Ra. ²³²Th was determined from ²²⁸Ac, and ²⁰⁸Tl using the 911.2 keV (intensity 25.8%) and 583.2 keV (intensity 84.5%) emission lines, respectively. ⁴⁰K was measured directly, using the 1460.8 keV emission line (intensity 10.7%). The specific activities of ¹³⁷Cs were also determined in the cases where it was detected using its 661.7 keV gamma emission peak.

Terrestrial gamma radiation (TGR) measurement

The gamma exposure rate at 1 m from the ground was measured in the center of each grid. The field detector used was a Ludlums μ R Model 12 S radiometer, which is a portable exposure rate detector based on sodium iodide doped with thallium, NaI(Tl), with a cylindrical sensitive detection volume of 2.5 cm radius by 2.5 cm height. It has a sensitivity of 175 cpm/ μ R/h and a linearity of around 10% of the actual measured value. This scintillation detector was selected due to the inherently high gamma-ray detection efficiency characteristic of this class of instruments. The detectors undergo regular calibration and verification to ensure measurement accuracy and stability.

This radiometer can be readily mounted on a tripod, enabling placement at a fixed height of 1 m above ground level. Maintaining a constant measurement geometry in this manner ensured homogeneous measurement conditions across all survey locations. Measurements were conducted in flat, unobstructed areas, avoiding slopes, ravines, dense vegetation, and water bodies, in accordance with CSN guidelines³⁹. In urban environments, measurements were kept at sufficient distances from paved surfaces and buildings; where this was not feasible, they were performed in the clearest accessible plots, positioned centrally and maximally distant from artificial structures.

A total of 47 TGR measurements were collected across the various field campaigns, corresponding to an average spatial density of approximately 3.8 data points per km². This density is substantially higher than that employed in the development of the Natural Gamma Radiation Map of Spain (MARNA) by the CSN for mainland Spain^{33,40}, where measurements were obtained at an average density of about 1.4 data points per 100 km².

To obtain the gamma dose rate from the experimental exposure-rate measurements, a conversion factor of $1 \mu R h^{-1} = 8.7 nGy h^{-1}$ was applied. To isolate the contribution due solely to gamma radiation from radionuclides in the ground (TGDR), the cosmic radiation component was subtracted from each experimental data point. The cosmic radiation component was estimated using the Eq. 9 proposed in the United Nations UNSCEAR 2000 report¹:

$$\dot{R}(z) = 26.1 [0.21e^{-1.65z} + 0.8e^{0.453z}] \quad (9)$$

where $\dot{R}(z)$ is the gamma dose rate due to cosmic background at the latitude of Melilla expressed in $nGy h^{-1}$ and z is the altitude in kilometres.

Geospatial analysis tools.

Spatial analyses of the variables measured in this study were carried out using Geographic Information System (GIS) software ArcGIS Pro, version 3.5 (ESRI²⁰). The generated maps provide a straightforward representation of the spatial distribution of the measured parameters across the study area. Spatial interpolation was performed using the Inverse Distance Weighted (IDW) method. This deterministic method applies weights to data points that are inversely proportional to the square of their distance from the prediction location. IDW is the default

interpolation option in ArcGIS and is one of the most commonly applied techniques in environmental studies for producing interpolated maps of radionuclide activity concentrations and related parameters^{41,42}.

Data availability

The datasets generated and/or analyzed during the current study are available from the corresponding author on reasonable request.

Received: 3 May 2025; Accepted: 9 January 2026

Published online: 22 March 2026

References

- Charles, M. *UNSCEAR report 2000: sources and effects of ionizing radiation. Journal Radiological Protection* **21** (2001).
- Eisenbud, M. & Gesell, T. F. *Environmental radioactivity: from natural, industrial, and military sources* (Elsevier, 1997).
- European Parliament. Council directive 2013/59/Euratom of 5 December 2013 laying down basic safety standards for protection against the dangers arising from exposure to ionising radiation, and repealing directives 89/618/Euratom, 90/641/Euratom, 96/29/Euratom, 97/43/Euratom a. *Off J. Eur. Commun.* **L13**, 1–73 (2014).
- Ministerio de la Presidencia, Relaciones con las Cortes y Memoria Democrática. Real Decreto 1029/2022 de 20 de diciembre, por el que se aprueba el Reglamento sobre protección de la salud contra los riesgos derivados de la exposición a las radiaciones ionizantes. 178672–178732 (2022).
- Gobierno de España. Código Técnico de la Edificación: Documento Básico HS. Sección HS 6: Protección frente al radón. Real Decreto 314/2006, de 17 de marzo (modificado por RD 732/2019). (2019).
- Hernandez, J., de Larouziere, F. D., Bolze, J. & Bordet, P. Le magmatisme neogene betico-rifain et Le couloir de décrochement trans-Alboran. *Bull. la. Société Géologique Fr.* **III**, 257–267 (1987).
- Hernández, J. & Bellon, H. Chronologie K-Ar du volcanisme miocène du Rif Oriental (Maroc): implications tectoniques et magmatologiques. *Rev. géologie Dyn. géographie Phys. Paris.* **26**, 85–94 (1985).
- El Bakkali, S., Gourgaud, A., Bourdier, J. L., Bellon, H. & Gundogdu, N. Post-collision neogene volcanism of the Eastern Rif (Morocco): magmatic evolution through time. *Lithos* **45**, 523–543 (1998).
- Duggen, S., Hoernle, K. & Van den Bogaard, P. Garbe-Schönberg, D. Post-Collisional transition from Subduction- to Intraplate-type magmatism in the Westernmost mediterranean: evidence for Continental-Edge delamination of Subcontinental lithosphere. *J. Petrol.* **46**, 1155–1201 (2005).
- UNSCEAR. *Ionizing Radiation: Sources and Biological effects. UNSCEAR 1982 Report To the General Assembly, with Annexes* (United Nations Publication, 1982).
- Sources, U. N. S. C. E. A. R. Effects and risks of ionizing Radiation. UNSCEAR 1988 report to the general Assembly, with annexes. *United Nations Publ* (1988).
- UNSCEAR. *Sources, Effects and Risks of Ionizing Radiation. UNSCEAR 2013 Report To the General Assembly, with Annexes* (United Nations Publication, 2013).
- Mabit, L., Benmansour, M. & Walling, D. E. Comparative advantages and limitations of the fallout radionuclides ¹³⁷Cs, ²¹⁰Pb_{ex} and ⁷Be for assessing soil erosion and sedimentation. *J. Environ. Radioact.* **99**, 1799–1807 (2008).
- Rodway-Dyer, S. J. & Walling, D. E. The use of ¹³⁷Cs to Establish longer-term soil erosion rates on footpaths in the UK. *J. Environ. Manage.* **91**, 1952–1962 (2010).
- Dueñas, C. et al. ⁷Be, ²¹⁰Pb and 40K depositions over 11 years in Málaga. *J. Environ. Radioact* **178–179**, 7, 325–334 (2017).
- Gaspar, L., Navas, A., Walling, D. E. & Machín, J. Gómez Arozamena, J. Using ¹³⁷Cs and ²¹⁰Pb_{ex} to assess soil redistribution on slopes at different temporal scales. *CATENA* **102**, 46–54 (2013).
- Peñuela, A. et al. A comparison of ²¹⁰Pb_{ex}, ¹³⁷Cs, and Pu isotopes as proxies of soil redistribution in South Spain under severe erosion conditions. *J. Soils Sediments.* **23**, 3326–3344 (2023).
- Behbehani, M., Uddin, S. & Baskaran, M. ²¹⁰Po concentration in different size fractions of aerosol likely contribution from industrial sources. *J. Environ. Radioact.* **222**, 106323 (2020).
- Biernacik, D. & Zalewska, T. ⁷Be, ²¹⁰Pb, airborne particulate matter and PM10 concentrations in relation to meteorological conditions in Southern Poland in 1998–2016. *J. Environ. Radioact.* **259–260**, 107122 (2023).
- Esri. ArcGIS Pro (version 3.5). Esri (2024).
- Saito, K. & Jacob, P. Gamma ray fields in the air due to sources in the ground. *Radiat. Prot. Dosimetry.* **58**, 29–45 (1995).
- Clouvas, A., Xanthos, S., Antonopoulos-Domis, M. & Silva, J. Monte Carlo calculation of dose rate conversion factors for external exposure to photon emitters in soil. *Health Phys.* **78**, 295–302 (2000).
- Quindos, L. S., Fernández, P. L., Ródenas, C., Gómez-Arozamena, J. & Arteché, J. Conversion factors for external gamma dose derived from natural radionuclides in soils. *J. Environ. Radioact.* **71**, 139–145 (2004).
- UNSCEAR. Sources and Effects of Ionizing Radiation. UNSCEAR 2000 Report to the General Assembly, with Scientific Annexes. vol. I. (2000).
- European Commission (EC). Radiological protection principles concerning the natural radioactivity of Building materials - Radiation protection 112. *Eur Comm* 1–16 (1999).
- García-Talavera, M. & López-Acevedo, F. J. Cartografía Del potencial de radón de España (Mapping Spain's radon potential). *Colección Inf. Técnicos del. Cons Segur Nucl* (2019).
- ICRP. 1990 Recommendations of the International Commission on Radiological Protection. ICRP Publication 60. *Ann. ICRP* **21**, (1991).
- Younis, H. et al. Gamma radioactivity and environmental radiation risks of granitoids in central and Western Gilgit-Baltistan, Himalayas, North Pakistan. *Results Phys.* **37**, 105509 (2022).
- Qureshi, A. A. et al. Evaluation of excessive lifetime cancer risk due to natural radioactivity in the rivers sediments of Northern Pakistan. *J. Radiat. Res. Appl. Sci.* **7**, 438–447 (2014).
- Briones, C. et al. Methodology for determination of radon prone areas combining the definition of a representative Building enclosure and measurements of terrestrial gamma radiation. *Sci. Total Environ.* **788**, 147709 (2021).
- Briones, C. et al. Multiparametric analysis for the determination of radon potential areas in buildings on different soils of volcanic origin. *Sci. Total Environ.* **885**, 163761 (2023).
- Briones, C. et al. Indoor radon risk mapping of the Canary Islands using a methodology for volcanic Islands combining geological information and terrestrial gamma radiation data. *Sci. Total Environ.* **922**, 171212 (2024).
- Quindós Poncela, L. S. et al. Natural gamma radiation map (MARNa) and indoor radon levels in Spain. *Environ. Int.* **29**, 1091–1096 (2004).
- García-Talavera, M., Matarranz, J. L., Martínez, M., Salas, R. & Ramos, L. Natural ionizing radiation exposure of the Spanish population. *Radiat. Prot. Dosimetry.* **124**, 353–359 (2007).
- Consejo de Seguridad Nuclear - CSN. Mapa de radiación gamma natural de España. (2001).
- Arnedo, M. A. et al. Mapping natural radioactivity of soils in the Eastern Canary Islands. *J. Environ. Radioact.* **166**, 242–258 (2017).

37. Consejo de Seguridad Nuclear - CSN. Procedimiento de toma de muestras para la determinación de la radiactividad en suelos: capa superficial. Colección Inf. Técnicos 11. Vigil. Radiológica Ambient. Proced. 1.1 (2003). (2003).
38. Suárez-Navarro, J. A., Moreno-Reyes, A. M., Gascó, C., Alonso, M. M. & Puertas, F. Gamma spectrometry and LabSOCS-calculated efficiency in the radiological characterisation of quadrangular and cubic specimens of hardened Portland cement paste. *Radiat. Phys. Chem.* **171**, 108709 (2020).
39. Herranz, M. *et al.* Procedimiento de muestreo y preparación de muestras para la determinación de la radiactividad en la capa superficial de los suelos. (2025). <https://www.csn.es/documents/10182/27786/INT-04-07+Vigilancia+radiológica+ambiental.+Procedimiento+1.1.+%28Rev.+1%2C+2025%29/e1dba231-7ad1-44ff-9afe-dfbf24c6ed56>
40. Suárez-Mahou, E. *et al.* INT-04-02 proyecto Marna. Mapa de radiación gamma natural.pdf. *Colección Informes Técnicos Consejo De Seguridad Nuclear* (2000).
41. Achilleos, G. A. The inverse distance weighted interpolation method and error propagation mechanism - creating a DEM from an analogue topographical map. *J. Spat. Sci.* **56**, 283–304 (2011).
42. Gong, G., Mattevada, S. & O'Bryant, S. E. Comparison of the accuracy of kriging and IDW interpolations in estimating groundwater arsenic concentrations in Texas. *Environ. Res.* **130**, 59–69 (2014).

Acknowledgements

Maps throughout this book were created using ArcGIS[®] software by Esri. ArcGIS[®] and ArcMap[™] are the intellectual property of Esri. All rights reserved. The lithostratigraphic maps were obtained from Cartografía Digital del Mapa Geológico y Continuo de España (GEODE) supplied by Instituto Geológico y Minero de España (IGME). The authors are particularly grateful to Luis Romero, Jose Antonio Hernández, M^a Paz Ojeda, Vicente de Juan and Santiago Cobreros for their continuous strong support in the field sampling campaigns and Eduardo González for his valuable suggestions regarding the statistical analysis of the data.

Author contributions

J.G. Rubiano conceived the study, wrote the main manuscript text, contributed to the discussion of results and conclusions, and participated in the sampling campaigns. F. Cámara was responsible for writing the geological section and discussing the results. N. Miquel-Armengol prepared the maps using ArcGIS and participated in data analysis. C. Briones developed the radon risk map section and revised the English language and bibliographic references. C. León-Navarro and M. Añino participated in the field sampling and in situ measurement campaigns. H. Alonso contributed to the discussion of the results. A. Tejera and P. Martel carried out the gamma spectrometry measurements of the soil samples, wrote the section on beaches, and contributed to the manuscript revision. J.G. Rubiano is the corresponding author.

Declarations

Competing interests

The authors declare no competing interests.

Additional information

Correspondence and requests for materials should be addressed to J.G.R.

Reprints and permissions information is available at www.nature.com/reprints.

Publisher's note Springer Nature remains neutral with regard to jurisdictional claims in published maps and institutional affiliations.

Open Access This article is licensed under a Creative Commons Attribution-NonCommercial-NoDerivatives 4.0 International License, which permits any non-commercial use, sharing, distribution and reproduction in any medium or format, as long as you give appropriate credit to the original author(s) and the source, provide a link to the Creative Commons licence, and indicate if you modified the licensed material. You do not have permission under this licence to share adapted material derived from this article or parts of it. The images or other third party material in this article are included in the article's Creative Commons licence, unless indicated otherwise in a credit line to the material. If material is not included in the article's Creative Commons licence and your intended use is not permitted by statutory regulation or exceeds the permitted use, you will need to obtain permission directly from the copyright holder. To view a copy of this licence, visit <http://creativecommons.org/licenses/by-nc-nd/4.0/>.

© The Author(s) 2026